Inorg. Chem. **2006**, *45*, 2866–2872

STM/STS Observation of Polyoxoanions on HOPG Surfaces: the Wheel-Shaped $[Cu_{20}Cl(OH)_{24}(H_2O)_{12}(P_8W_{48}O_{184})]^{25-}$ and the Ball-Shaped $[\{Sn(CH_3)_2(H_2O)\}_{24}\{Sn(CH_3)_2\}_{12}(A\text{-}PW_9O_{34})_{12}]^{36-}$

Mohammad S. Alam,[†] Viacheslav Dremov,[†] Paul Müller,*[,†] Andrei V. Postnikov,[§] Sib Sankar Mal,[‡] Firasat Hussain,[‡] and Ulrich Kortz*[,‡]

Physikalisches Institut III, Universität Erlangen-Nürnberg, Erwin-Rommel-Strasse 1, 91058 Erlangen, Paul Verlaine University - LPMD/IPC, 1 Bd. Arago, F-57078 Metz, France, and Institute of Metal Physics, S. Kowalewskoi 18, 620219 Yekaterinburg, Russia, School of Engineering and Science, International University Bremen, P.O. Box 750 561, 28725 Bremen, Germany

Received September 15, 2005

A combination of scanning tunneling microscopy (STM) and scanning tunneling spectroscopy (STS) techniques have been performed on the wheel-shaped $[Cu_{20}Cl(OH)_{24}(H_2O)_{12}(P_8W_{48}O_{184})]^{25-}$ and the ball-shaped $[\{Sn(CH_3)_2(H_2O)\}_{24}\{Sn(CH_3)_2\}_{12}(A\text{-}PW_9O_{34})_{12}]^{36-}$ deposited on highly oriented pyrolytic graphite surfaces. Small, regular molecule clusters, as well as separated single molecules, were observed. The size of the molecules is in agreement with the data determined by X-ray crystallography. In STS measurements, we found a rather large contrast at the expected location of the Cu metal centers in our molecules, i.e., the location of the individual Cu ions in their organic matrix is directly addressable by STS.

Introduction

The scanning tunneling microscope has become an important tool to image surfaces with atomic resolution.[1] There has been particular interest in recent years to obtain images of individual molecules adsorbed on surfaces, even if these substances are insulating in their bulk structure.[2,3] Many insulating materials have been successfully imaged using scanning tunneling microscopy (STM) by depositing these materials on conductive substrates.[4] Particularly polyoxometalates (POMs) which form self-assembled monolayers, as well as individual species, in a periodic arrangement on different substrates were imaged by STM at small bias voltages.[4−9] This is surprising since the gap energy between highest occupied molecular orbitals (HOMOs) and lowest unoccupied molecular orbital (LUMO) of the isolated molecules is relatively large. One possible explanation of this type of imaging could be the decrease of the HOMO−LUMO energy gap due to molecule−molecule or molecule−substrate interactions.[10]

Although STM is capable of atomic resolution when imaging solid surfaces, mapping of large, complex molecules with submolecular resolution is a difficult task. An STM image contains both geometric and electronic information about the sample in a complicated way.[11−13] Even highly resolved STM topography images cannot provide information about specific features of large molecules. As, for example,

* To whom correspondence should be addressed. Tel: (+49) 9131-85-27073. Fax: (+49) 9131-15249. E-mail: phm@physik.uni-erlangen.de.
[†] Universität Erlangen-Nürnberg.
[§] University of Metz and Institute of Metal Physics.
[‡] International University Bremen.

(1) Binnig, G.; Rohrer, H.; Gerber, C.; Weibel, E. *Phys. Rev. Lett.* **1982**, *49*, 57.
(2) Chiang, S. in: Güntherodt, H. J., Wiesendanger, R., Eds. *Scanning Tunneling Microscopy I*; Springer-Verlag: Berlin, 1992; p 182.
(3) Jung, T. A.; Himpsel, F. J.; Schlittler, R. R.; Gimzewski, J. K. In *Scanning Probe Microscopy*; Wiesendanger, R., Ed.; Springer-Verlag: Berlin, 1998; p 11.
(4) Song, I. K.; Shnitser, R. B.; Cowan, J. J.; Hill, C. L.; Barteau, M. A. *Inorg. Chem.* **2002**, *41*, 1292.
(5) Song, I. K.; Barteau, M. A. *Kor. J. Chem. Eng.* **2002**, *19*, 567.
(6) Song, I. K.; Lyons, J. E.; Barteau, M. A. *Catal. Today* **2003**, *81*, 137.
(7) Kaba, M. S.; Song, I. K.; Duncan, D. C.; Hill, C. L.; Barteau, M. A. *Inorg. Chem.* **1998**, *37*, 398.
(8) Song, I. K.; Kaba, M. S.; Barteau, M. A. *Langmuir* **2002**, *18*, 2358.
(9) Kaba, M. S.; Song, I. K.; Barteau, M. A. *J. Phys. Chem. B* **2002**, *106*, 2337.
(10) Fisher, A. J.; Blochl, P. E. *Phys. Rev. Lett.* **1993**, *70*, 3263.
(11) Paz, O.; Brihuega, I.; Gómez-Rodríguez, J. M.; Soler, J. M. *Phys. Rev. Lett.* **2005**, *94*, 056103.
(12) Feyter, S. D.; Schryver, F. C. D. *J. Phys. Chem. B* **2005**, *109*, 4290.
(13) Hembacher, S.; Giessibl, F. J.; Mannhart, J. *Phys. Rev. Lett.* **2005**, *94*, 056101.

10.1021/ic051586z CCC: $33.50
Published on Web 03/11/2006

we would scan the van der Waals surface of large and complex molecules, we would see only a featureless "blob" of a large cluster of atoms. However, spectroscopic possibilities of STM allow us to probe electronic states of the molecules as a function of energy.[14,15] If there would be subunits of the molecule exhibiting a special type of chemical bonding, STM spectroscopy would allow for filtering out special features of the species if they arise at energies well separated from the other states of the molecule.

POMs are early-transition-metal oxygen clusters with an enormous variety of shapes, sizes, and composition.[16] This class of compounds (often described as soluble metal-oxide fragments) has received increasing attention recently, mostly due to its multitude of interesting catalytic, electronic, magnetic, medicinal, thermal, and optical properties.[16]

Recently, two of us reported on the synthesis of an unprecedented Cu_{20}-containing polyoxotungstate of large size and high symmetry by self-assembly techniques making use of the template effect.The wheel-shaped $[Cu_{20}Cl(OH)_{24}(H_2O)_{12}(P_8W_{48}O_{184})]^{25-}$ (**$Cu_{20}P_8W_{48}$**) represents the first transition metal-substituted derivative of $[H_7P_8W_{48}O_{184}]^{33-}$ and incorporates more Cu^{2+} ions than any other polyoxometalate known to date.[17] The electrochemistry properties of **$Cu_{20}P_8W_{48}$** have also been reported.[18]

Two of us also reported on unprecedented polyoxotungstates with spectacular size (almost 1000 atoms), molar mass (~33 000 g/mol) and symmetry (ball-shaped) which have been synthesized by nano-molecular self-assembly techniques.[19] The dimethyltin-substituted $[\{Sn(CH_3)_2(H_2O)\}_{24}\{Sn(CH_3)_2\}_{12}(A\text{-}XW_9O_{34})_{12}]^{36-}$ (X = P, **$Sn_{36}P_{12}W_{108}$**; As, **$Sn_{36}As_{12}W_{108}$**) consist of twelve (A-XW_9O_{34}) Keggin moieties linked by 36 dimethyltin groups resulting in a spherical structure with an 8 Å cavity.

The objective of this present work is to achieve topographic, as well as spatially resolved, electronic structural information of **$Cu_{20}P_8W_{48}$** and **$Sn_{36}P_{12}W_{108}$**. STM and scanning tunneling spectroscopy (STS) were performed on single molecules adsorbed onto highly oriented pyrolytic graphite (HOPG). Several groups have reported formation of ordered and monolayer arrays of POMs on surfaces and have imaged these using STM.[4−9,20,21] However, in our case, we concentrate on isolated, free-standing single molecules in order to find out specific features of the electronic properties at the single-molecule level. Recently, the investigations on specific functionalities of molecular nanostructures at surfaces have been reviewed.[22,23] STS measurements are very often carried out under ultrahigh vacuum conditions combined with low temperatures to increase the signal-to-noise ratio.[24] However, it has been shown that under certain conditions STM experiments are also capable to detect local electronic properties at room temperature.[25]

In the work reported here, we used a home-built scanning tunneling microscope working under ambient conditions. As our STM head was optimized for very low drift, we succeeded to combine high-resolution topography mapping with simultaneous current−voltage characteristics (STS) measurements on single polyanion molecules deposited on HOPG surfaces. HOPG is one of the best studied substrate concerning its electronic properties both experimentally and theoretically.[26] In this study, individual polyanion molecules were observed with submolecular resolution. In particular, in **$Cu_{20}P_8W_{48}$**, the Cu metal centers were visualized using the STS technique.

Experimental Section

Polyoxoanion Synthesis. The polyanions **$Cu_{20}P_8W_{48}$** and **$Sn_{36}P_{12}W_{108}$** were prepared according to the published procedures.[17,19]

STM Experiments. A homemade scanning tunneling microscope was used for measurements. The microscope was equipped with a commercially available low-current control system (RHK Technology). Samples of **$Cu_{20}P_8W_{48}$** and **$Sn_{36}P_{12}W_{108}$** on HOPG were conveniently prepared by allowing aqueous solutions to evaporate under air. Concentrations were between 10^{-8} and 10^{-10} M at pH 4−6. Before adding the solution onto the substrate surface, we ensured that the tunneling tip had a sufficiently high resolution. We calibrated distances in the STM images by observing atomic spacing on HOPG. Typically, for the STM measurements, tunneling currents between 5 and 200 pA were employed. The bias voltage was ±50 to ±500 mV. The scan frequency was varied between 2 and 5 Hz. Resolution was 256 × 256 points for topography, and 128 × 128 points in the STS measurements. STS studies have been performed in the current-imaging tunneling spectroscopy mode (CITS) simultaneously with constant current image by the interrupted-feedback-loop technique. This was carried out by opening

(14) Novokmet, S.; Alam, M. S.; Dremov, V.; Heinemann, F. W.; Müller, P.; Alsfasser, R. *Angew. Chem., Int. Ed.* **2005**, *44*, 803.

(15) Ako, A. M.; Maid, H.; Sperner, S.; Zaidi, S. H. H.; Saalfrank, R. W.; Alam, M. S.; Müller, P.; Heinnemann, F. W. *Supramol. Chem.* **2005**, *17*, 315.

(16) (a) Pope, M. T. *Heteropoly and Isopoly Oxometalates*; Springer-Verlag: Berlin, 1983. (b) Pope, M. T.; Müller, A. *Angew. Chem., Int. Ed. Engl.* **1991**, *30*, 34. (c) *Polyoxometalates: From Platonic Solids to Anti-Retroviral Activity*; Pope, M. T., Müller, A., Eds.; Kluwer: Dordrecht, The Netherlands, 1994. (d) *Chemical Reviews, Polyoxometalates*; Hill, C. L., Ed.; 1998. (e) *Polyoxometalate Chemistry: From Topology via Self-Assembly to Applications*; Pope, M. T., Müller, A., Eds.; Kluwer: Dordrecht, The Netherlands, 2001. (f) *Polyoxometalate Chemistry for Nano-Composite Design*; Yamase, T., Pope, M. T., Eds.; Kluwer: Dordrecht, The Netherlands, 2002. (g) Pope, M. T. *Comput. Coord. Chem. II* **2003**, *4*, 635. (h) Hill, C. L. *Comput. Coord. Chem. II* **2003**, *4*, 679. (i) *Polyoxometalate Molecular Science*; Borrás-Almenar, J. J., Coronado, E., Müller, A., Pope, M. T., Eds.; Kluwer: Dordrecht, The Netherlands, 2004. (j) Casan-Pastor, N.; Gomez-Romero, P. *Fron. Biosci.* **2004**, *9*, 1759.

(17) Mal, S. S.; Kortz, U. *Angew. Chem., Int. Ed.* **2005**, *44*, 3777.

(18) Jabbour, D.; Keita, B.; Nadjo, L.; Kortz, U.; Mal, S. S. *Electrochem. Comm.* **2005**, *7*, 841.

(19) Kortz, U.; Hussain, F.; Reicke, M. *Angew. Chem., Int. Ed.* **2005**, *44*, 3773.

(20) Errington, R. J.; Petkar, S. S.; Horrocks, B. R.; Houlton, A.; Lie, L. H.; Patole, S. N. *Angew. Chem.* **2005**, *117*, 1280.

(21) Keita, B.; Nadjo, L. *Surf. Sci.* **1991**, *254*, L443.

(22) De Feyter, S.; De Schryver, F. C. *Chem. Soc. Rev.* **2003**, *32*, 139.

(23) Samorì, P. *Chem. Soc. Rev.* **2005**, *34*, 551.

(24) (a) Ho, W. J. *Chem. Phys.* **2002**, *117*, 11033. (b) Wahl, P.; Diekhöner, L.; Schneider, M. A.; Vitali, L.; Wittich, G.; Kern, K. *Phys. Rev. Lett.* **2004**, *93*, 176603.

(25) (a) Miura, A.; Chen, Z.; Uji-i, H.; De Feyter, S.; Zdanowska, M.; Jonkheijm, P.; Schenning, A. P. H. J.; Meijer, E. W.; Würthner, F.; De Schryver, F. C. *J. Am. Chem. Soc.* **2003**, *125*, 14968. (b) Gesquière, A.; De Feyter, S.; De Schryver, F. C.; Schoonbeek, F.; van Esch, J.; Kellogg, R. M.; Feringa, B. L. *Nano Lett.* **2001**, *1*, 201. (c) Jäckel, F.; Watson, M. D.; Müllen, K.; Rabe, J. P. *Phys. Rev. Lett.* **2004**, *92*, 188303.

(26) Matsui, T.; Kambara, H.; Niimi, Y.; Tagami, K.; Tsukada, M.; Fukuyama, H. *Phys. Rev. Lett.* **2005**, *94*, 226403.

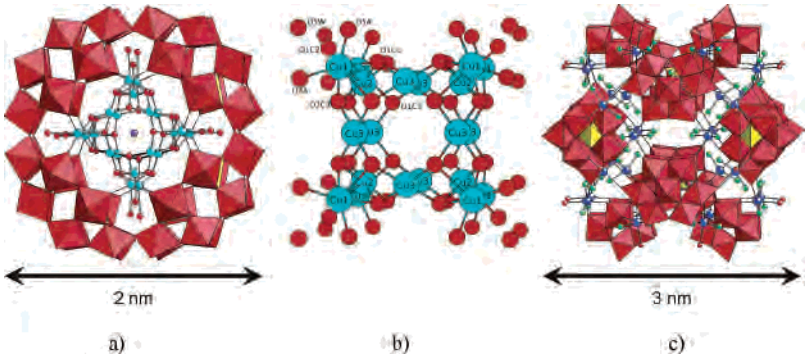

Figure 1. (a) Combined polyhedral/ball-and-stick representation of **$Cu_{20}P_8W_{48}$**. The color code is as follows. Copper (turquoise), oxygen (red), and chlorine (violet). The WO_6 octahedra are red, and the PO_4 tetrahedra are yellow. (b) Ball-and-stick representation of the copper-hydroxo cluster in **$Cu_{20}P_8W_{48}$** showing all structurally equivalent copper atoms with the same label. The labels refer to the DFT calculations of Figure 6. The cluster is rotated by 45° relative to Figure 1a. (c) Combined polyhedral/ball-and-stick representation of **$Sn_{36}P_{12}W_{108}$**. The labeling scheme is as follows. Tin (blue), oxygen (red), and carbon (green). The WO_6 octahedra are red, and the PO_4 tetrahedra are yellow.

the feedback loop to fix the separation between the tip and sample and ramping of the bias voltage over the range of interest. The scan range of voltages was typically from −1 to 0.1 V relative to the tip potential for 113 discrete voltage steps. Typically, tunneling resistances on the order of 5 GΩ were set. We used Pt−Ir (90/10) tips mechanically cut from wires with a diameter of 0.25 mm.

Results and Discussion

Polyanion Structures. The polyanion **$Cu_{20}P_8W_{48}$** represents the first transition metal-substituted derivative of $[H_7P_8W_{48}O_{184}]^{33-}$, and it incorporates more Cu^{2+} ions than any other polyoxometalate known to date. The structure of the wheel-shaped $[H_7P_8W_{48}O_{184}]^{33-}$ precursor is maintained in **$Cu_{20}P_8W_{48}$**, and the cavity has been filled with a highly symmetrical copper-hydroxo cluster (see Figure 1a). The Cu_{20} cluster in **$Cu_{20}P_8W_{48}$** is composed of only three structurally unique types of copper(II) ions (8 Cu1, 4 Cu2, and 8 Cu3), see Figure 1b. All 20 copper centers are bridged to neighboring copper ions via μ_3-oxo ligands, resulting in a highly symmetrical, cagelike assembly. Interestingly, the center of the cavity (which has a diameter of around 7 Å) is occupied by a chloride ion (see Figure 1a). The coordination numbers and geometries of Cu1, Cu2, and Cu3 are different from each other. Cu1 is coordinated in a strongly distorted octahedral fashion and exhibits Jahn−Teller distortion with axial elongation. The equatorial plane is composed of Cu1−O3A (1.922(14) Å), Cu1−O5A (1.926(15) Å), Cu1−O2C3 (1.980(14) Å), and Cu1−O1Cu (1.986(14) Å) bonds. The two axial bonds are Cu1−O1C3 (2.358(16) Å) and a very long bond Cu1−O5W (2.504(17) Å) to a terminal water molecule. The angle O1C3−Cu1−O5W is only 145°, which reflects steric hindrance for the latter. Cu2 has square-pyramidal coordination geometry with two Cu2−O2C3 (1.922(14) Å) and two Cu2−O1Cu (1.925(14) Å) bonds in the equatorial plane and a long bond to a terminal water ligand, Cu2−O1C2 (2.29(3) Å). Finally, Cu3 has a square-planar coordination geometry which is composed of Cu3−O1C3 (1.905(16) Å), Cu3−O1Cu (1.933(14) Å), Cu3−O1C3′ (1.947(16) Å), and Cu3−O2C3 (1.948(14) Å) bonds. The copper−copper distances in **1** are as follows. Cu1···Cu2, 2.812(3) Å; Cu1···Cu3, 3.045(4) Å; and Cu1···Cu3′, 3.052(4) Å.

The polyanion **$Sn_{36}P_{12}W_{108}$** exhibits a spherical structure which is spectacular in terms of geometry and size (diameter of ∼30 Å), see Figure 1c. An additional attractive feature is the 8 Å cavity in the center of the molecule. The whole molecular assembly of **$Sn_{36}P_{12}W_{108}$** is composed of 12 trilacunary $[A\text{-}XW_9O_{34}]^{9-}$ (X = P, As) Keggin fragments which are linked by a total of 36 dimethyltin groups (12 inner $(CH_3)_2Sn^{2+}$ and 24 outer $(CH_3)_2(H_2O)Sn^{2+}$ groups), resulting in a polyanion with T_h symmetry. Interestingly, **$Sn_{36}P_{12}W_{108}$** has almost 1000 atoms and a molar mass of around 33 000 g/mol. In addition, 14 cesium ions are closely associated with **$Sn_{36}P_{12}W_{108}$** in the solid state. They are located in hydrophilic surface pockets of the spherical clusters, thereby stabilizing the assembly further. Polyanion **$Sn_{36}P_{12}W_{108}$** represents the second largest, discrete polyoxotungstates ever reported.

STM Results on $Sn_{36}P_{12}W_{108}$. The molecular structure of **$Sn_{36}P_{12}W_{108}$** is represented in Figure 1c. Molecular ordering on a surface is controlled by a delicate balance between intermolecular forces and molecule−substrate interactions. As the bonding of the complex molecules to the substrate is weak, diffusion is possible along the surface. The mobility is reduced at defects, e.g., monatomic graphite steps. Thus, an aggregation of molecules is to be expected, particularly in such places. At very dilute conditions, the polyanions get trapped along the steps of the HOPG surface. High-resolution STM images with increasing magnification of **$Sn_{36}P_{12}W_{108}$** are depicted in Figure 2. The images reveal the well-ordered distribution of **$Sn_{36}P_{12}W_{108}$** even at room temperature. The molecules are aligned along the graphite steps in a linear fashion. Individual molecules were clearly distinguished and mapped. Figure 2a−c shows a linear molecule arrangement with increasing magnification. In Figure 2c, even the graphite substrate is mapped with atomic resolution next to a single molecule. The periodicity of the molecules is about 11.4 nm, which is much higher than the intermolecular distance of 3.2 nm determined from the X-ray structure.[19] The size of a single molecule in the STM images is in accordance with the molecular diameter of approximately 3 nm[19] (see Figure 1c). The distorted hexagonal

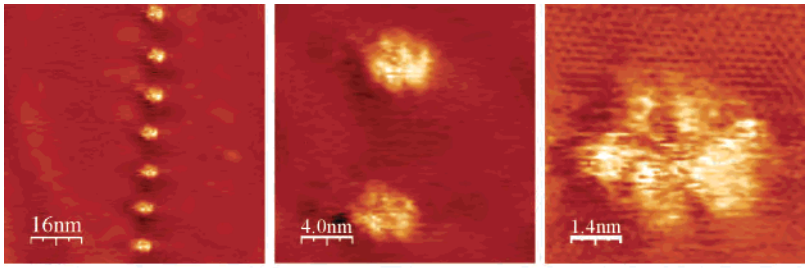

Figure 2. (a−c) Constant-current STM topographies with increasing magnifications of the ball-shaped $\mathbf{Sn_{36}P_{12}W_{108}}$ on a HOPG surface. At low concentrations, there are linear superstructures of $\mathbf{Sn_{36}P_{12}W_{108}}$. For (a) and (b), the set-point current was 5 pA and the set-point voltage was 100 mV; for (c), the set-point current was 200 pA and the set-point voltage was −400 mV.

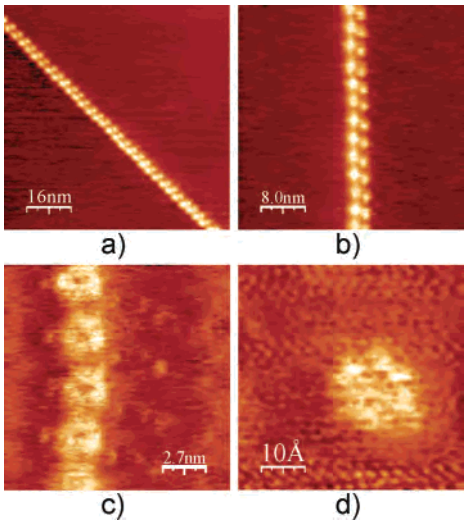

Figure 3. STM images of wheel-shaped $\mathbf{Cu_{20}P_8W_{48}}$ molecules deposited onto a HOPG surface. (a) and (b) At low concentrations, we observe double-linear superstructures of $\mathbf{Cu_{20}P_8W_{48}}$ aligned along graphite steps (set-point current 5 pA, set-point voltage 100 mV). (c) Formation of highly regular, 1D molecular arrangements. The wheel shape of $\mathbf{Cu_{20}P_8W_{48}}$ is clearly discernible. (d) An isolated $\mathbf{Cu_{20}P_8W_{48}}$ molecule with submolecular resolution. The background shows the underlying graphite with atomic resolution (set-point current 200 pA, set-point voltage −200 mV).

shape is reminiscent to the overall shape of the molecule, as illustrated in the projection in Figure 1c.

In our STS measurements of $\mathbf{Sn_{36}P_{12}W_{108}}$ (picture not shown), we see only faint features in the range of bias voltages between + 1.0 and −1.0 V, i.e., in the region of levels around the Fermi level. These features show a hexagonal shape similar to the STM topography measurements. However, without having detailed theoretical calculations, we cannot ascribe them to any specific group of atoms in the molecule (see our discussion of the $Cu_{20}P_8W_{48}$ molecule below).

STM Results on $\mathbf{Cu_{20}P_8W_{48}}$. The data presented in Figure 3 show regular patterns of well-ordered arrays of $\mathbf{Cu_{20}P_8W_{48}}$ on the graphite surface. The polyanion molecules are nicely aligned along the substrate step-edges or other defects of the HOPG surface.

There are several types of polyanion arrangements on the HOPG surface depending on the concentration of the $\mathbf{Cu_{20}P_8W_{48}}$ solution, which can be observed after repeated scanning with relatively mild tunneling conditions. Double linear structures were formed at the graphite steps (Figure 3a and b). At very low molecular coverages, 1D ordered arrangements (Figure 3c) are found even at room temperature. Figure 3d shows a high-resolution STM image of a single $\mathbf{Cu_{20}P_8W_{48}}$ molecule. In the background, one can see clearly the atomic resolution of graphite. The polyanion molecule appears to be slightly elongated due to the drift of the STM head. After correction for this, the $\mathbf{Cu_{20}P_8W_{48}}$ molecule appears cyclic with a diameter of about 2.3 nm, which is consistent with the maximum diameter derived from X-ray diffraction data.[17]

STS Results on $\mathbf{Cu_{20}P_8W_{48}}$. To achieve a better understanding of how STM images are related to the geometric and electronic structure of the deposited $\mathbf{Cu_{20}P_8W_{48}}$ ion arrays, we also performed spatially resolved CITS of this polyanion. We restricted our measurements to negative potentials of the substrate relative to the tip. CITS has been developed for STS of a sample surface.[28,29] CITS involves the measurement of the $I-V$ characteristics at each pixel of the normal STM topography. The tip-to-sample distance is defined by the topography parameters. One then has a normal STM topography image, as well as current images, where the current images are obtained from the three-dimensional data set of $I(V, x, y)$. The current image thus represents a slice, at a given voltage, of the tunneling current as a function of the lateral x, y coordinates. Variations on this scheme can be performed whereby $I-V$ characteristics are recorded at a subset of points in a grid or along a particular line in an image. The current contrast changes significantly when at certain bias voltages new molecular energy levels come into play, thus enhancing the information obtained from topography alone. Therefore, this type of current imaging measurements allows spatially resolved energy spectroscopy.[30] The CITS technique has been applied successfully to semiconductor materials, but its application to organic molecules is rather difficult because of mobility or instability of the molecules, drift, etc.[31]

With our home-built low-drift STM head, we successfully applied this technique to $\mathbf{Cu_{20}P_8W_{48}}$. We were able to

(27) Klusek, Z.; Kozlowski, W. *J. Electron Spectrosc. Relat. Phenom.* **2000**, *107*, 63.
(28) Hamers, R. J.; Tromp, R. M.; Demuth, J. E. *Phys. Rev. Lett.* **1986**, *56*, 1974.
(29) Alam, M. S.; Strömsdörfer, S.; Dremov, V.; Müller, P.; Kortus, J.; Ruben, M.; Lehn, J. M. *Angew. Chem. Int. Ed.* **2005**, *44*, 7896.
(30) *Scanning Tunneling Microscopy*; Stroscio, J. A., Kaiser, W. J., Eds.; Academic Press: New York, 1993.
(31) Rivera, M.; Williamson, R. L.; Miles, M. J. *J. Vac. Sci. Technol. B* **1996**, *14*, 1472.

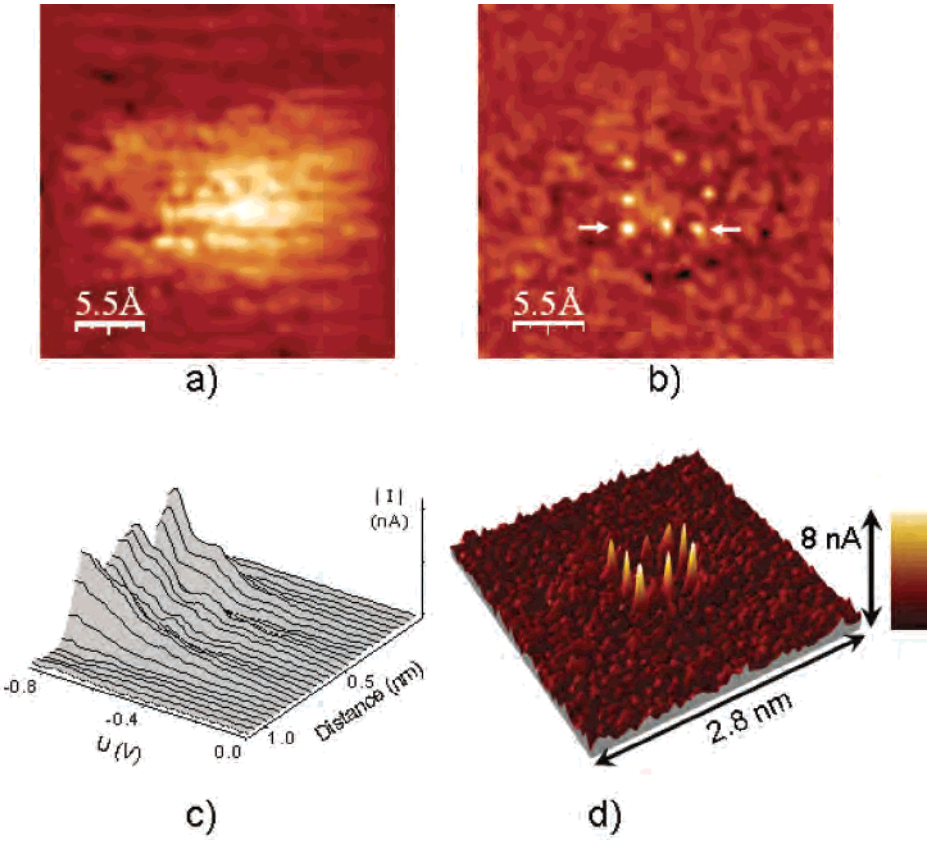

Figure 4. (a) Topography image of $\mathbf{Cu_{20}P_8W_{48}}$. (b) Simultaneously recorded CITS current image taken at a voltage of −0.913 V. A quadratic array of bright spots is clearly seen. The distance between the spots is approximately 0.28 nm. (c) Set of $I-V$ characteristics taken at positions between the two arrows in (b). (d) Filtered perspective 3D representation of the CITS image in (b).

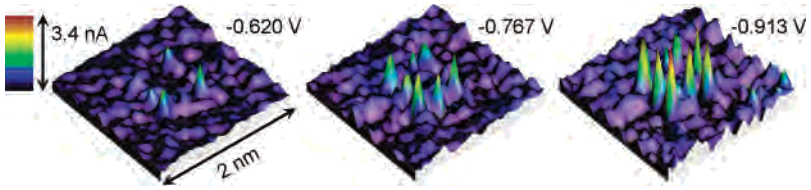

Figure 5. Set of 3D current images from the same scan as in Figure 4. The background current is subtracted.

visualize structures conforming in their distances to those of the Cu···Cu distances. Figure 4a shows the topography imaging together with a simultaneously measured CITS image (Figure 4b) taken at a bias voltage of −0.913 V. The tip-to-sample distance was defined by a low-voltage tunneling resistance of 5 GΩ. The topographic image presents a rather washed-out sphere with some faint brighter spots. The diameter is approximately 2.1 nm, which conforms to the outer diameter of the wheel-shaped $\mathbf{Cu_{20}P_8W_{48}}$. However, in the CITS image (Figure 4b), one recognizes a quadratic array of eight bright spots which represent sharp peaks of the tunneling current. This can be seen even more clearly in the perspective 3D representation of the CITS map in Figure 4d. We associate the peaks with the images of the Cu atoms in the orientation as in Figure 1b. As in this projection, the Cu1 and Cu2 atoms in the corners are rather close to each other, we assume that they are mapped only as one single spot. The average distance between neighboring peaks is 0.28 nm, conforming well to the distances of 0.27 nm between the average position of the projection of Cu1 and Cu2 and the Cu3 position, as obtained from X-ray diffraction (Figure 1a and b).[17] In Figure 4c, a 3D current profile is taken at 30 equidistant positions between the two arrows of the current image in Figure 4b. The background current arising from the HOPG surface has been subtracted. There are three ridges, and the distances between neighboring ridges are approximately 0.3 nm. We note that there is a steep current increase at voltages below −0. 4 V (Figure 4). Despite the high resolution of the current images (Figures 2 and 3), no remarkable features arising from the μ_3-oxo ligands were detectable.[27] We observed only a faint signal next to the Cu cluster from the rest of the molecule. In our discussion of Figure 4c, we mentioned already that below a threshold of approximately −0.4 V the tunneling current at the positions of the bright spots increases drastically. This can be seen more clearly in the set of 3D current maps presented in Figure 5. The data were recorded in the same scan as in Figure 4. We conclude that we have mapped local maxima of the density of states (DOS) at the position (of the projection to the plane) of the Cu atoms. Therefore, it is rather interesting to compare these experimental results with the electronic structure of the molecule.

Theoretical Calculations

A useful insight into the origins of the maxima present in the STS images may be delivered from first-principle calculations of the electronic structure. These calculations have been done in the framework of the density functional theory (DFT) using the method and computer code Siesta[32] with strictly confined numerical atom-centered basis functions. The polyanion $\mathbf{Cu_{20}P_8W_{48}}$ crystallizes in a tetragonal lattice with 25 potassium and lithium cations. Skipping them, along with crystalline water, but otherwise keeping all atoms and bondings within the polyanion, we treated the latter in our calculation as an isolated fragment, charged 25−. We emphasize that there was neither a substrate included in our calculation nor an explicit treatment of the electron transport. We attempt to draw certain conclusions based on the analysis of the electron density distribution within the energy window accessible to the experiment. Technically, the calculation in Siesta always involves a simulation box, which is defined in order to perform the Fourier transformation of charge density. In our case, this simulation box had a size of 30 × 30 × 30 Å^3, large enough to avoid the interaction with repeated "images" of the polyanion across the cell boundary.

We are aware that Heisenberg model simulations of the magnetic structure of $\mathbf{Cu_{20}P_8W_{48}}$ are underway,[33] but so far, no definite information about the magnetic structure is available to us. We tested several configurations and singled out the one with the lowest total energy for the subsequent discussion. In this configuration, eight Cu3 ions at the edges of the inner cube ordered their spins antiferromagnetically, whereas each of the Cu1−Cu2−Cu1 "trimers" decorating the faces of the Cu3 cube exhibited parallel setting of Cu 1/2 spins within it. The cumulative spins of two (opposite) trimers were set antiparallel to the other two, which resulted in a $S = 0$ configuration of the polyanion. Local magnetic moments (and local densities of states) were not much affected by an inversion of some spins at the Cu sites, as follows from electronic structure calculations for several other trial configurations. The magnitudes of the Cu magnetic moments were found to be about $\pm 0.5\ \mu_B$, i.e., smaller than the expected 1 μ_B for a Cu^{2+} ion, due to hybridization with neighboring oxygen atoms. However the "magnetization cloud" associated with each Cu atom (or, correspondingly, with the Cu trimers) extends over their neighboring oxygen atoms. Therefore, a nominal spin $S = 1/2$ per each Cu atom is recovered in a rather delocalized fashion.

Figure 6 shows the local densities of states at several sites in the polyanion. An energy gap of 0.08 eV separates the HOMO (of mostly Cu3d−O2p character) from the LUMO, which is of almost exclusively Cu3d character. It follows from the calculation that the molecular orbitals situated within an energy window of 0.9 eV below the chemical potential would have a substantial contribution from the 3d states of the Cu1−Cu2−Cu1 trimers but only a rather small

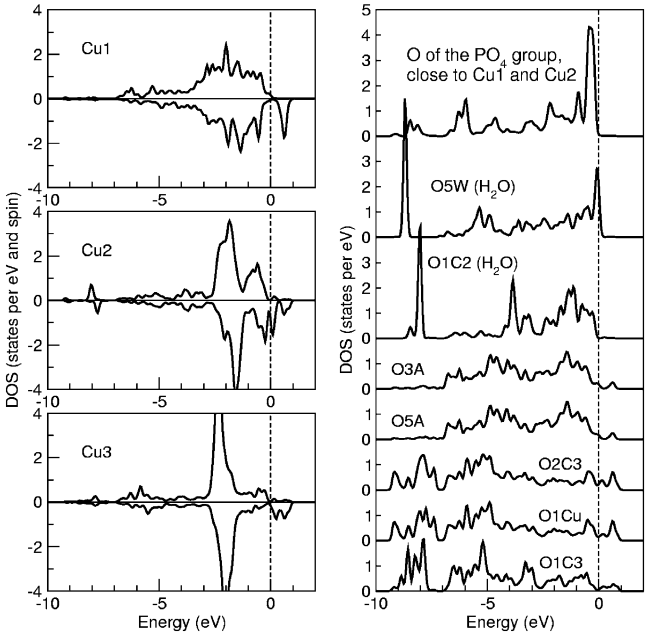

Figure 6. Local DOS at three different Cu sites (left panel) and at eight different O sites (right panel) of the 25− charged Cu_{20} polyanion obtained from the DFT calculation. The labeling is explained in Figure 1b. The dashed line at 0 eV separates occupied and vacant states. The continuous DOS was obtained from broadening the discrete energy levels of the isolated molecular fragment with a width parameter of 0.1 eV. See text for details.

one from the cube-edge Cu3 atoms. Moreover, the 2p states of the oxygen atoms within the PO_4 groups and the water molecules close to the Cu trimers would provide an essential contribution within this energy window. This is quite different from what is seen in the experimental STS (CITS) images (Figures 4b and 5), where the contribution from all Cu atoms is present with similar intensity, with no intensity seen at the positions of the oxygen atoms.[34] However, within 0.9 eV above the chemical potential, the unoccupied states are of about equal intensity for all Cu atoms, and exclusively for them, i.e., there is no contribution from any of the oxygen sites. Figure 7a shows the electron density of unoccupied states, integrated over an energy interval of 0.9 eV above the chemical potential.

As the substrate potential was always negative with respect to the tip, one would expect only probing of the occupied levels because electrons are extracted from the molecule. However, as soon as there is a substantial energy barrier between substrate and molecule, the potential of the molecule is "sweeping" between the ones of substrate and tip. The exact alignment of the molecular levels relative to the chemical potentials of substrate or tip depends sensitively on the heights of the barriers between substrate and molecule and between molecule and tip. In fact, it is influenced rather delicately by the charge balance between molecule and substrate, as well as by the distance between the tip and the

(32) Soler, J. M.; Artacho, E.; Gale, J. D.; García, A.; Junquera, J.; Ordejón, P.; Sánchez-Portal, D. *J. Phys.: Condens. Matter* **2002**, *14*, 2745; http://www.uam.es/siesta/.

(33) Allalen, M.; Schnack, J., private communication.

(34) It could be added that a notably insufficient inclusion of Coulomb correlation effects in a conventional DFT calculation like the present one cannot be responsible for the discrepancy observed. Namely, the qualitative effect of stronger Coulomb correlation within the quite localized Cu 3d shell is predictable. It would be the shift of the occupied Cu d levels downward, enhancing the O 2p character in the highest occupied states.

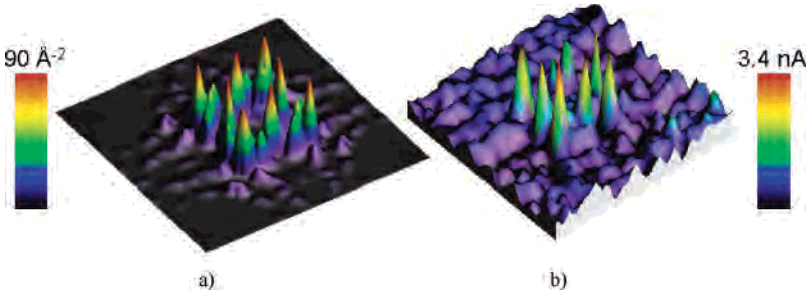

Figure 7. (a) 3d representation of the calculated electron density, integrated over an energy interval of 0.9 eV above the chemical potential and along the *z* axis throughout the molecule. (b) The similarity to the experimental CITS image obtained at a bias of −0.913 V is striking (see Figure 5).

molecule.[35] It is easy to recognize that tunneling via the unoccupied levels is possible even if the electron transport goes from the substrate via the molecule into the tip. In our case, by varying the initial voltage and current settings, we varied the tip-to-molecule distance such that we obtained maximum contrast in the CITS images. An inspection of the DFT results shows that the maximum contrast between Cu-related (i.e., the eight-dot array seen in Figures 4b and 5) and not-Cu-related contributions might be achieved if we probe the lowest unoccupied levels, which are the vacant Cu d states. We state that this heuristic method works only if there is an exclusive contribution of a highly symmetrically distributed species, as is the case with the 3d levels of the Cu ions. To emphasize the adequacy of our interpretation of STS images through the involvement of unoccupied states, we show in Figure 7a the calculated electron density, integrated over an energy interval of 0.9 eV above the chemical potential and along the *z* axis throughout the molecule. The similarity to the measured STS data at a bias of −0.913 V is striking (Figure 7b, see also Figure 5).

Generally, one would assume that the weakest bonds, i.e., in our case the coordinate-covalent bonds of the Cu ion, should dominate the molecular orbitals near the Fermi level of the molecule because this type of bonds has the lowest ionization energy. Therefore, in this sense, STS spectroscopy directly addresses the metal centers. As we have found, a similar behavior for the Co centers in supramolecular [2 × 2] grid molecules[29] or for the Fe ions in ferric wheels,[15] it is reasonable to assume that we can locate any weakly bond metal center in rather complex molecules.

(35) Lindsay, S. *J. Chem. Educ.* **2005**, *82*, 727.

Conclusions

STM and CITS images of the large, wheel-shaped $\mathbf{Cu_{20}P_8W_{48}}$ and the very large, ball-shaped $\mathbf{Sn_{36}P_{12}W_{108}}$ were observed on HOPG surfaces at room temperature. Ordered lines, as well as individual molecules, were observed with submolecular resolution. The so-determined molecular dimensions of the individual polyanion molecules were in good agreement with X-ray crystallography data. Individual Cu metal centers were visualized using the STS spectroscopy technique. Local DOS measurements shows that the sharp peaks in the CITS images define the positions of the Cu atoms. This is in good agreement with the results of a DFT calculation of the unoccupied levels.

Acknowledgment. U.K. and F.H. thank the International University Bremen, and S.S.M. thanks the Deutsche Forschungsgemeinschaft (SPP 1137) for research support. P.M. acknowledges financial support by SFB 583, Deutsche Forschungsgemeinschaft. A.V.P. thanks the Deutsche Forschungsgemeinschaft (SPP 1137) for providing computational facilities and thanks J. Schnack and M. Allalen for the introduction into the $\mathbf{Cu_{20}P_8W_{48}}$ problematic and for numerous useful discussions. Figure 1 was generated by Diamond Version 3.1a (copyright Crystal Impact GbR). Figures 2, 3, 4a, 4b, and 5 were generated by WSxM [Nanotec Electrónica, Madrid].

IC051586Z